1-1-2023

Role of air staging in a batch-type fixed bed biomass combustor under constant primary air

Awais Junejo
Edith Cowan University

Yasir M. Al-Abdeli
Edith Cowan University

Jacobo Porteiro

10.1007/s11630-023-1869-9
Junejo, A., Al-Abdeli, Y. M., & Porteiro, J. (2023). Role of air staging in a batch-type fixed bed biomass combustor under constant primary air. Journal of Thermal Science. Advance online publication. https://doi.org/10.1007/s11630-023-1869-9

Journal of Thermal Science

https://doi.org/10.1007/s11630-023-1869-9

Role of Air Staging in a Batch-Type Fixed Bed Biomass Combustor under Constant Primary Air

Awais JUNEJO[1*], Yasir M. AL-ABDELI[1], Jacobo PORTEIRO[2]

1. School of Engineering, Edith Cowan University, Joondalup, WA 6027, Australia
2. CINTECX Universidade de Vigo, Grupo de Tecnoloxia Enerxética (GTE) 36310 Vigo, España

Abstract: Staged combustion of biomass is the most suitable thermo-chemical conversion for achieving lower gaseous emissions and higher fuel conversion rates. In a staged fixed bed combustion of biomass, combustion air is supplied in two stages. In the first stage, primary air is provided below the fuel, whereas in the later stage, secondary air is supplied in the freeboard region. The available literature on the effects of air staging (secondary air location) at a constant primary air flow rate on combustion characteristics in a batch-type fixed bed combustor is limited and hence warrants further investigations. This study resolves the effect of air staging, by varying the location of secondary air in the freeboard at five secondary to total air ratios in a batch-type fixed bed combustor. Results are reported for the effects of these controlled parameters on fuel conversion rate, overall gaseous emissions (CO_2, CO and NO_x) and temperature distributions. The fuel used throughout was densified hardwood pellets.

Results show that a primary freeboard length (distance between fuel bed top and secondary air injection) of 200 mm has higher fuel conversion rates and temperatures as well as lower CO emissions, at a secondary to total air ratio of 0.75 as compared to primary freeboard length of 300 mm. However, NO_x emissions were found to be lower for a primary freeboard length of 300 mm as compared to 200 mm. An increase in secondary to total air ratio from 0.33 to 0.75 resulted in higher freeboard temperatures and lower CO as well as NO_x emissions. The outcomes of this study will be helpful in the effective design of commercial scale biomass combustors for more efficient and environmentally friendly combustion.

Keywords: fixed bed combustor, biomass combustion, air staging, freeboard temperature, burning rate, gaseous emissions

1. Introduction

Combustion of fossil fuels, such as coal, is the main cause of various detrimental environmental effects such as acid rain, air and water pollution and it significantly contributes to CO_2 emissions, a greenhouse gas leading to global warming [1, 2]. Besides increasing CO_2 concentration in the environment, the coal combustion also results in emissions of sulphur, which itself causes acid rain [3, 4]. In this scenario, renewable energy sources such as biomass can be a solution to these problems [5, 6]. Biomass is a carbon-neutral energy

Received: Nov 17, 2022
AE: YANG Bin

Corresponding author: Awais JUNEJO
E-mail: ajunejo@our.ecu.edu.au

Nomenclature:

A	Cross sectional area of fuel bed and combustor/m^2	Q_t	Total air flowrate (Q_s+Q_p)/kg·m^{-2}·s^{-1}
BR	Burning rate/kg·m^{-2}·s^{-1}	Q_s/Q_t	Secondary to total air ratio
D	Combustor internal diameter/mm	t	Time/s
d	Distance between two adjacent fuel bed thermocouples/mm	Δt	Time interval/s
FBT	Fuel Bed Temperature/°C	W	Width/mm
IFV	Ignition front velocity/mm·s^{-1}	X_{CO}	Carbon monooxide concentration/10^{-6}
L_I	Primary freeboard length/mm	X_{CO_2}	Carbon dioxide concentration/%
L_{II}	Secondary freeboard length/mm	X_{NO_x}	Nitrogen Oxide concentration/10^{-6}
Δm	Mass decrement/kg	X_{O_2}	Oxygen concentration/%
Q_p	Primary air flowrate/kg·m^{-2}·s^{-1}	x	Distance from fuel bed top at the start of experiment/mm
Q_s	Secondary air flowrate/kg·m^{-2}·s^{-1}		

source, having zero net CO_2 emissions and negligible sulphur content [7, 8]. Direct combustion of biomass is most suitable thermo-chemical conversion and accounts for 95% of the global biomass usage [9]. The size of biomass based direct combustion plant varies from small size to large scale commercial power plant [10, 11]. Smaller size plants are mainly of fixed bed configurations and are primarily used for lab-based research and domestic heating. These small size plants are of counter-current type and incorporate stationary grates [12]. Laboratory scale fixed bed combustors feature widely in the literature due to their effectiveness in analyzing the process and fuel conversion efficiency of large commercial scale moving grate combustors [13, 14].

The fuel bed arrangement used in the present study follows counter-current configuration in which the flame front propagates downward opposite to the (upward) primary air flow [14–17]. Experiments to determine the optimum primary to secondary air ratio in lab-scale systems become key in identifying the optimal operating conditions of commercial systems. Whilst many studies have dealt with air staging effects, in batch-type as well as continuous feed fixed bed biomass combustors [18–20], no studies have ventured into changing secondary air (Q_s) stoichiometry, and its location relative to fuel bed, whilst keeping primary air (Q_p) constant in a batch-type combustor. The significance of the latter is that it allows for the sensitivity of secondary air (location, stoichiometry) to be studied, whilst the packed bed stoichiometry remains the same. It also means the likely effects of secondary air jets, injected just above the fuel bed, can be more clearly understood compared to other investigations in which primary (Q_p) and secondary air (Q_s) might have been varied simultaneously. With this in mind, the current study examines effects of primary freeboard length (distance of secondary air location from fuel bed) and secondary to total air ratio whilst keeping primary air flow rate fixed. In this manner, the exact role of secondary air staging and its proximity to the top of the fuel bed, can be resolved. This study is continuation of previous work [18] that also investigated the effects of primary freeboard length, in which total air (Q_t=Q_p+Q_s) was constant and primary as well as secondary air was varied.

The combustion of biomass results in a number of continuous heterogeneous and homogeneous reactions. Along with its useful power, biomass combustion results in the generation of ash and emissions. Apart from high ash content, moisture contents, cellulose/lignin ratio and calorific value are also some of the challenges associated with the use of biomass as a fuel. In this regard, many different treatment processes are being developed to improve the physical and chemical properties of biomass [21–24]. Further, the lower thermal efficiency of biomass combustion plants is also an issue which results in lower process temperatures and higher concentration of carbon monoxide [25–28]. A solution to these problems can be modification or improvements in operational parameters such as air preheating, air staging and pre-treatment of fuel. Moreover, improving the thermal efficiency of biomass combustion plants [25–28] relies on an improved understanding of the way in which primary air and secondary air independently affect the overall fuel conversion efficiency and the resulting emissions. Yet, Table 1 which summarises most work carried out on air stagging using lab-scale biomass combustors shows that in all the cases, both the primary and secondary air were simultaneously varied. Keeping total air constant and varying both primary and secondary air may not give a clear idea of the effect that secondary air flow and its location have on overall combustion characteristics. Whilst air staging has previously been shown to influence emissions [29] and in particular primary air is known to influence fuel burning rate, fuel bed

Table 1 Experimental studies into air staging strategies in fixed bed biomass combustors

Combustor type	Column length, L/mm	D or W/ mm	Constant Q_p	Flow rate/ kg·m^{-2}·s^{-1}	Biomass fuel type	Reference
Continuous feed (fuel bed does not move)	1500	1300	No	0.01–0.05	Pellets/densified	[33]
	1500	120		0.06–0.09		[20]
	1500	120		0.07–0.11		[34]
	1500	120		0.04–0.15		[35]
Batch-type (fuel bed moves downward)	320	120	No	0.16–0.50	Chips/non-densified	[19]
	890	206		0.21–0.54		[36]
	1700	200		0.03–0.08	Pellets/densified	[28]
	1500	202		0.19–0.35		[18, 37]

temperatures and emissions. A higher primary air flow (near or above stoichiometric condition) can result in greater particulate matter as well as NO_x emissions. Therefore, in staged combustion, primary air is mainly supplied less than stoichiometric condition in the range of 30% to 60% of stoichiometric air [12, 20]. Accordingly, unburned hydrocarbons leaving the packed bed during the fuel's devolatization phase are thermally converted in the freeboard region after mixing with secondary air.

There is a realisation for the need to better understand, and independently study the secondary air (location, stoichiometry) due to its effect on reducing CO as well as NO_x emissions by 50% and 37%, respectively compared to non-staged operation (Q_s=0) [30]. Further to this, Deng et al. [19] showed that by varying the primary and secondary air flow rates, the fuel burning rate can be improved by providing a Q_s/Q_t of 0.60. Similarly, Zadravec et al. [31] investigated the effect of air staging (primary to secondary air ratio) and excess air on sensible heat loss and gaseous emissions in a laboratory scale wood pellet boiler. The results show that a low primary to secondary air ratio of 0.53 results in reduction of NO_x and CO emissions by 14.4% and 93.9% respectively. A significant reduction in CO emissions (approximately 41%) at a primary to secondary air ratio of 0.20 was also observed by Collodo et al. [32], who investigated combustion characteristics of olive cake in a fixed bed combustor. Some studies have investigated the influence of change in primary freeboard length on combustion characteristics. However, these studies have not been performed under constant primary air operations. For varied primary air operations, an increase in Q_s/Q_t results in lower primary air and greater secondary air flow rate. Due to this, any increase or decrease in investigated parameters can be either due to a decrease in primary air or an increase in secondary air. Therefore, to provide a clear indication of the effect of secondary air on combustion performance, the current study investigates the effect of change in primary freeboard length at a constant primary air.

Despite the availability of extensive literature on the combustion of biomass in fixed bed configurations, studies on the effect of secondary location inside a combustor (primary freeboard length) and secondary flow rate on combustion characteristics such as fuel conversion, fuel bed and freeboard temperatures, as well as emissions, are scarce. The effects of primary freeboard length on combustion characteristics using the same batch-type fixed bed combustor as of current study were investigated previously at varied primary air [18]. The current study will further explore the findings from previous work on the effect of primary freeboard length at a constant primary air. With the above in mind, the main objectives of current study focus on the two main areas of biomass combustion in a fixed bed combustor:

Fuel bed: To investigate the in-bed combustion characteristics; burning rate, ignition front velocity and fuel bed temperature at a constant primary air whilst varying secondary air flow rate (Q_p=0.08 kg·m^{-2}·s^{-1} and Q_s=0.04–0.26 kg·m^{-2}·s^{-1}) at two primary freeboard lengths of L_l=200 mm and 300 mm.

Freeboard: To analyse the role of varying primary freeboard length at L_l=200 mm (L_l/D=1.00) and L_l=300 mm (L_l/D)=1.48 on freeboard temperatures and gaseous emissions (CO_2, NO_x and CO).

Benefits from this study help in the selection of operating conditions (primary and secondary air flow rate) and in the designing (secondary air location) for more efficient and less polluting biomass combustion systems.

2. Methodology

This section presents the details of type of combustor and fuel used as well as the methods used for obtaining the temperature, emissions and fuel mass loss data. Details about the post-processing of data can be found elsewhere [38].

2.1 Fixed bed combustor and data acquisition

Fig. 1 shows sectional and assembly views of the biomass combustor operating on a counter-current

configuration [18]. It features, from the lower end, a primary air plenum, column with various thermocouple and fuel supply ports, a top flange through which exhaust gases move upwards into the extraction system and the secondary air penetrates downwards into the column. The freeboard region is broken down into two zones; the primary freeboard, the region starting from the fuel bed surface to secondary air injection point, and the secondary freeboard which is the remainder of the column towards the top flange. The combustor has an internal diameter (D) of 202 mm and length (L) of 1500 mm and is manufactured using stainless steel. The ratio of the combustor diameter to the equivalent particle diameter was 31 corresponding to D/L of 0.13 as seen in Table 1 whereby at this ratio wall effects can be neglected [39]. A stainless-steel fuel grate with an open area of 32% was placed 100 mm above the plenum using a variable height spacer. Two plenum side ports were used to supply the primary air.

The distance between the primary air inlet and fuel grate was approximately 150 mm. The purpose of this distance was to allow a more uniform flow of primary air to the fuel bed. A distance of 150 mm was sufficient to allow a uniform supply of primary air to the fuel grate as shown in Fig. S1 of the supplementary materials. A further decrease in distance between primary air inlet and fuel grate might result in a non-uniform supply of primary air which can result in channelling of fuel bed [40]. Whereas, a greater distance between primary air inlet and fuel grate results in a shorter freeboard length of the combustor. Due to the high volatile content of biomass, a longer residence time in the freeboard is required for complete combustion. Therefore, a shorter freeboard length and residence time can result in incomplete combustion and higher CO emissions [41]. Additionally, flow conditioning was applied to the plenum for flow uniformity. The secondary air assembly is combination of a downpipe and a circular ring with eight holes, each of 3 mm in diameter. The downpipe is attached to the combustor's top flange. The length of the downpipe inside the combustor can be adjusted to the desired level. The position (distance) of the secondary air with respect to the top of the packed bed (L_{I}) and the secondary freeboard length (L_{II}) can be modified for a given total freeboard length ($L_{\mathrm{I}} + L_{\mathrm{II}}$) by varying the length of downpipe inside the combustor. Additionally, the primary and secondary freeboard lengths can also be varied, by using a spacer to elevate the fuel bed into the combustor column thereby reducing the total length of freeboard ($L_{\mathrm{I}} + L_{\mathrm{II}}$) from its design length of 1500 mm.

Data from eleven thermocouples, positioned axially along the centreline of the freeboard and packed bed, were acquired at a rate of 0.2 Hz using National Instruments thermocouple module (model: NI 9213) and data acquisition system (model: cRIO-9074XT). Thermocouples were of N-type. Table S1 of the supplementary materials shows the axial location of all fuel bed and freeboard thermocouples. The sheath diameter and the length of the thermocouple were 3 mm and 300 mm respectively. With a resolution of 0.15°C, the thermocouples can measure temperature in the range of –270°C to 1300°C. Stainless steel compression fittings were used while mounting the thermocouples on combustor wall to avoid heat loss and leakage of flue gases.

A Testo 350 X/ML gas analyser was used to measure gaseous emissions (CO, CO_2, NO_x, and O_2). Concentration of gaseous emissions in the flue gas was measured just above the exhaust pipe of the combustor.

Emissions data presented in later parts of this study were obtained during the steady state operation of the combustor. Further details about identification of onset of steady state can be observed in Figs. S2 and S3 (Supplementary materials). The applied gas analyser has a resolution of 1.0×10^{-6} for NO emissions levels up to 3.0×10^{-3}, 0.1×10^{-6} for NO_2 for emissions levels up to 5.0×10^{-4}, and 0.01% for CO_2 and O_2. Similar to previous studies conducted on biomass combustion, concentrations of CO_2, NO_x and CO in the flue gas were corrected to a baseline 10% of O_2 as per ASTM standard of flue and exhaust gas analysis PTC 19.10 using Eq. (1) [20, 42–44].

$$X_{\mathrm{O_2,ref}} = X_{\mathrm{O_2,measured}} \frac{21-[\mathrm{O_2,ref}]}{21-[\mathrm{O_2,measured}]} \quad (1)$$

where X is the gas concentration in vol% (CO_2, NO_x and CO); the subscript "O_2,ref" is the baseline oxygen concentration for calculating X (10% of O_2); the subscript "O_2, measured" is measured value of gas concentration corresponding to oxygen concentration measured during the experiment. The conversion of gaseous species to a baseline 10% of O_2 allows comparison of results obtained from the current study and earlier works carried out at a similar operating condition.

2.2 Biomass fuel and combustion conditions

Hardwood pellets (make: Maxiheat Hard Wood Pellets) were utilised as a fuel. The diameter and nominal length of the pellets was 6.5 mm and 5–40 mm respectively. ASTM standards [45–48], were used to perform the proximate and ultimate analysis of the fuel. Bulk density of pellets was measured as per ASTM E873 [49]. Table 2 lists the proximate and ultimate analysis of the fuel which is pictured (as received state) in Fig. 1.

The fuel batch used for each experiment was 3.9 kg, which resulted in fuel bed height of approximately 150–165 mm. After charging the combustor with the desired amount of fuel, 15 mL of methylated spirt

(concentrated 96% ethanol) was sprayed on fuel bed surface, which was then ignited using a handheld butane flame torch. Each test was repeated three times. The primary freeboard length was varied (200 mm and 300 mm) at a constant secondary freeboard length of 700 mm. This was achieved by using two spacers of 300 mm and 550 mm in height. This is emphasised as the main feature of the current study, as variations in primary freeboard length and secondary air flow rate are not dependent of secondary freeboard length and primary air flow. Primary freeboard lengths of 200 and 300 mm were selected due to their better combustion characteristics identified in previous work [18]. After igniting the fuel, the flow of primary and secondary air was increased slowly upto the desired level. Data acquisition (Fuel bed temperatures, freeboard temperatures, emissions and mass deficit) started once the desired flow rates of primary and secondary air were achieved.

Table 2 Proximate and ultimate analysis of pellets

Parameter	Value
Proximate analysis	
Volatile matter[a]/% (in weight)	78.4
Fixed carbon[a]/% (in weight)	14.1
Ash/% (in weight)	0.86
HHV[a]/MJ·kg^{-1}	19.1
Unit density/kg·m^{-3}	1165
Bulk density/kg·m^{-3}	713.4
Ultimate analysis	
Carbon/%	45.8
Hydrogen/%	5.3
Oxygen/%	48.8

a: Dry basis.

2.3 Fuel conversion

Determining the instantaneous fuel conversion rate requires real-time measurement of fuel consumption. In order to acquire a time-series of (instantaneous) fuel mass loss throughout the duration of each experiment, the whole combustor assembly was attached to a hydraulic lift platform with an integral load cell. The load cell was in the form of an industrial scale (make: Wedderburn, model; SUK300), with a capability to measure the mass upto 300 kg and sensitivity of 100 grams (equivalent to 0.0014 m^3 of fuel bed volume). A digital indicator (make: Rinstrum, model: RAR320A) was used to record the data from load cell via its Rinstrumview software. During testing, the lift platform carrying the load cell was elevated to carry the entire weight of the combustor. At the conclusion of each experiment, the lift platform was lowered thereby allowing the combustor to instead bear its entire weight on a floor-affixed steel frame, as seen in Fig. 1. In this manner, the load cell was only loaded during testing.

Whilst the lift platform was raised carrying the combustor, burning rate (kg·m^{-2}·s^{-1}) of the fuel was calculated using mass deficit of fuel throughout the steady state regime. The burning rate (BR) was used to express the rate of fuel conversion relative to the cross-sectional area of the fuel bed as presented in Eq. (2).

$$\mathrm{BR} = \frac{\Delta m}{\Delta t \cdot A} \tag{2}$$

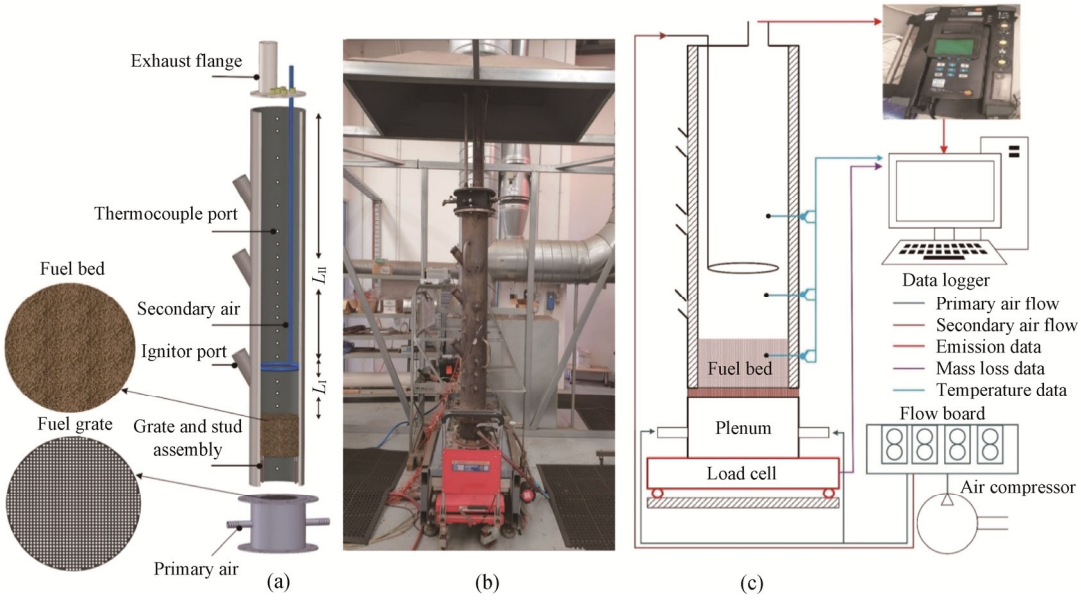

Fig. 1 Biomass combustor: (a) sectional view, (b) as operated in the lab and (c) data acquisition set-up

Table 3 Combustion conditions used

Primary freeboard length, L_f/ mm	L_f/D	Primary Air, Q_p		Secondary Air, Q_s/		Total Air, Q_t/	Q_s/Q_t	Uncertainty/ %
		kg·m^{-2}·s^{-1}	L/min	kg·m^{-2}·s^{-1}	L/min	kg·m^{-2}·s^{-1}		
200	1.00	0.089	140	0.044	70	0.134	0.33	±5**
				0.089	140	0.179	0.50	
				0.134	210	0.224	0.60*	
				0.179	280	0.269	0.66	
				0.224	350	0.313	0.71	
				0.269	420	0.358	0.75	
300	1.48	0.089	140	0.044	70	0.134	0.33	±5**
				0.089	140	0.179	0.50	
				0.134	210	0.224	0.60*	
				0.179	280	0.269	0.66	
				0.224	350	0.313	0.71	
				0.269	420	0.358	0.75	

*: Instability case; **: Full scale reading.

The method used here provides a direct, and more accurate measure of the fuel conversion rate compared to other values for BR found in the literature [50–52]. Most of the previous research uses the data from fuel bed thermocouple data to obtain the ignition front velocity (IFV) in mm·s^{-1}, which can be used to calculate burning rate (BR=IFV×ρ_{fuel}). That alternate approach is largely used for simplicity as it negates the need for real-time fuel conversion measurements. However, the use of IFV (fuel bed temperature data) to obtain BR does not account the mass of char left in the combustor, which can lead to an overestimation of fuel burning rate in comparison to direct measurement of fuel mass loss specially at lower air flow rates [53]. A comparison between BR obtained using fuel mass loss and IFV can be observed in Fig. S4 (Supplementary materials). However, fuel bed temperature data were also utilized to find the IFV. IFV was calculated by considering the time taken by the ignition front (t) to reach a specific pre-determined reference temperature between two adjacent thermocouples that are located at a distance (d) from each other (Eq. (3)). The distance (d) between two adjacent fuel bed thermocouples (TC2 and TC1) in the present work was 50 mm. Theoretically, any temperature can be used as a reference temperature to calculate time taken by ignition front; a temperature value of 600°C for estimating IFV was considered as a reference temperature, the same temperature value was also considered in previous studies [39, 54].

$$IFV = d/t \quad (3)$$

The primary air flow rate was selected less than stoichiometric air (in this case stoichiometric conditions occurs at Q_t=0.358 kg·m^{-2}·s^{-1} or 560 L/min) to avoid higher particulate and gaseous emissions [18]. Secondary air flow rate was then increased in equal steps until total air flow rate became 560 L/min (stoichiometric condition). Further details about experimental setup and methods used can be found elsewhere [18, 37]. Total errors associated with the experimental data are displayed in Tables S2 and S3 (Supplementary Materials). A more detailed description of experimental conditions is listed in Table 3.

3. Results and Discussion

In order to examine the influence of primary freeboard length and secondary air flow rate on fuel conversion, freeboard temperatures and emissions for the experimental conditions listed in Table 3, this section initially investigates the effect of these variables on fuel bed temperatures and burning rates. This section then presents data related to freeboard temperatures and emissions. The data for the Q_s/Q_t=0.60 (Q_s=0.134 kg·m^{-2}·s^{-1}) case were not presented here, as this case was subject to instabilities. The instabilities were found to occur at certain primary freeboard lengths (200 mm–550 mm) and secondary air flow rates in the range of 0.224 kg·m^{-2}·s^{-1} to 0.269 kg·m^{-2}·s^{-1}. The occurrence of instabilities increased with the increase in primary freeboard length, i.e. 400 mm and 550 mm [37]. This can be due to the fact that the secondary air is located at a more distant location from the fuel bed in these cases and the temperature of unburned volatiles emitted from the fuel bed decreases by the time they reach the secondary air. In addition to the lower temperature of volatiles, a higher secondary air flowrate causes quenching due to convective cooling and results in incomplete combustion and instabilities. Apart from the incomplete combustion

of the post fuel bed volatiles, the mechanisms leading to occurrence of instabilities could also be caused by the thermo-acoustic coupling due to the variation in temperature distributions along the combustor length and warrants further investigation. Further detail about the occurrence of the instabilities can be found elsewhere [37]. Primary freeboard lengths greater than 300 mm in addition to more instable conditions, also resulted in lower combustion temperatures and higher gaseous emissions [18]. Therefore, only two primary freeboard lengths of L_l=200 mm and 300 mm were selected.

3.1 Fuel bed conversion rates and temperatures

Figs. 2 and 3 show the time series of fuel bed thermocouples at different values of Q_s/Q_t for L_l/D=1.00 and 1.48. Fuel bed thermocouples TC1 and TC2 were located at 50 mm and 100 mm respectively, below the top of the fuel bed at the start of the experiment. However, TC3 was placed at the top of fuel bed. It can be observed from Figs. 2 and 3 that Q_s/Q_t has minimal effect on the magnitude of fuel bed temperature for both L_l/D=1.00 and 1.48. Fuel bed temperature slightly increased from 790°C to 908°C for L_l/D=1.00 and from 796°C to

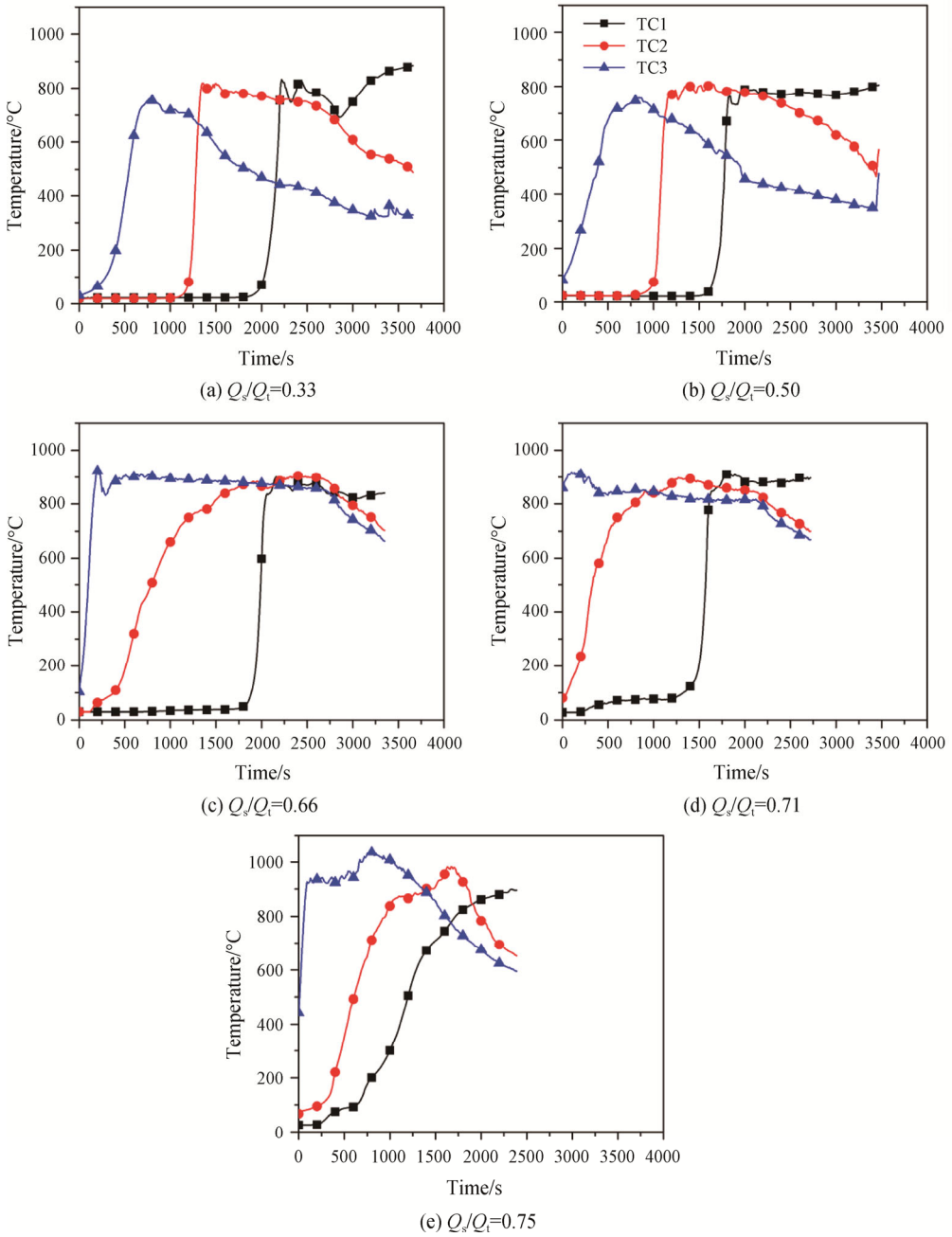

Fig. 2 Fuel bed thermocouple time series for L_l/D=1.00

893°C for L_l/D=1.48 as the Q_s/Q_t increased from 0.33 to 0.75. This rise was around 14% and 12% for L_l/D=1.00 and 1.48 respectively, as shown in Table 4. Further, the peak fuel bed temperatures were similar for L_l/D=1.00 and 1.48 at all the values of Q_s/Q_t tested i.e. 790°C (L_l/D=1.00) and 796°C (L_l/D=1.48) at Q_s/Q_t=0.33 and 893°C (L_l/D=1.00) and 908°C (L_l/D=1.00) at Q_s/Q_t= 0.75. Fuel bed temperatures are mainly affected by primary air flow rate [18, 50]. Therefore, no significant difference in peak fuel bed temperatures for L_l/D=1.00 and 1.48, can be due to the use of the constant primary air flow rate in the current study. Whilst increase in peak fuel bed temperatures with the increase in Q_s/Q_t can be due to increased drying of fuel at greater values of Q_s/Q_t=0.66, 0.71 and 0.75. However, a significant difference in trends of TC1 and TC2 for L_l/D=1.00 and 1.48 was observed at Q_s/Q_t=0.66, 0.71 and 0.75 cases. Fuel bed temperature for TC2, as observed in Fig. 3, rose sharply from ambient temperature as the ignition front reached the thermocouple for L_l/D=1.48 at all Q_s/Q_t tested. Further, the ignition front then propagated downwards toward the next thermocouple in the fuel bed (TC1) which also follows the same trend. However, for L_l/D=1.00, value of fuel bed temperature as observed from TC2 rose much

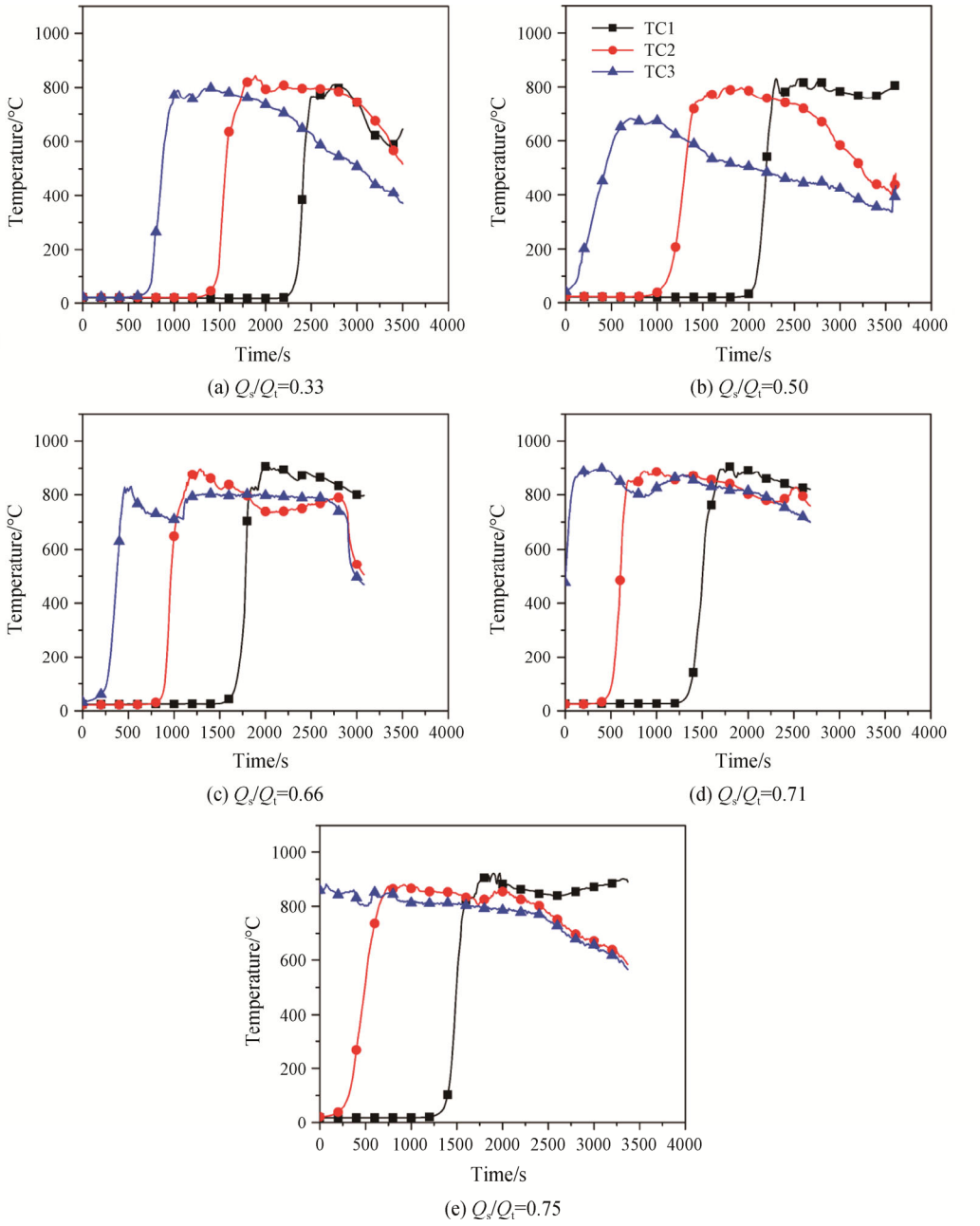

Fig. 3 Fuel bed thermocouple time series for L_l/D = 1.48

earlier than ignition front arrival at Q_s/Q_t=0.66 and for both TC1 and TC2 at Q_s/Q_t=0.71 and 0.75. For L_l/D=1.00 at Q_s/Q_t=0.75, the temperature inside the fuel bed was around 200°C at 500 s, which increased slowly and reached a peak temperature of 850°C (when the front reached the thermocouples) at 2000 s as seen in Fig. 2. This behaviour was only noticed for L_l/D=1.00 at greater Q_s/Q_t values.

This behaviour can be related to the lower distance of secondary air from the fuel bed, i.e., 200 mm, which despite having very high flow rates at Q_s/Q_t=0.66, 0.71 and 0.75, did not quench the reactions happening inside the bed, but rather instead helped the burning process. Higher secondary flow rate due to greater value of Q_s/Q_t of 0.66, 0.71 and 0.75 corresponding to secondary air flow rate of 0.296, 0.313 and 0.358 kg·m^{-2}·s^{-1}, increased the heat transfer from the top combusting part of the fuel bed to the lower layers of the fuel bed, which were not combusted yet, leading to a rise in temperature of lower layers. The rise of fuel bed temperature above 100°C for L_l/D=1.00 case, caused drying of fuel, which eventually increased the burning rate as the burning rate of wood pellets is higher for fuels with lower moisture content [55]. Interestingly, at Q_s/Q_t=0.66, higher temperature before ignition front arrival is only observed for TC2. Additionally, the rise in temperature of TC2 (located near the top surface of the fuel bed) at Q_s/Q_t=0.66 can be attributed to a lower secondary flowrate corresponding to 0.266 kg·m^{-2}·s^{-1} as compared to 0.313 kg·m^{-2}·s^{-1} and 0.358 kg·m^{-2}·s^{-1} at Q_s/Q_t=0.71 and 0.75. This flow rate is not enough to transfer the heat from the ignition front located at the top surface of the fuel bed to bottom layers of fuel (where TC1 is located). As the secondary air flowrate increases further in the case of Q_s/Q_t=0.71 and 0.75, heat transfer from the top surface of fuel bed is enhanced by strong downward penetrating secondary air jets and therefore, this rises the temperature of TC1 before the arrival of ignition front. Furthermore, increased radiative heat transfer from the uppermost layers of the fuel bed also results in a rise in the temperature of TC1 due to an increase in fuel bed temperature at higher values of Q_s/Q_t=0.71 and 0.75 as seen in Table 4.

Fuel conversion rates (BR and IFV) initially decreased with rise in Q_s/Q_t from 0.33 to 0.66. Increasing Q_s/Q_t further to 0.75, resulted in higher fuel conversion rate for both L_l/D=1.00 and 1.48. This increment in fuel conversion rates was more significant for L_l/D=1.00 as compared to L_l/D=1.48, especially at Q_s/Q_t=0.75. The increase in fuel conversion rates (BR and IFV) for Q_s/Q_t= 0.71 and 0.75 cases can be attributed to the greater values of temperatures for the lower portion of the fuel bed (TC1) which removes moisture from fuel (causing drying) in these two conditions before the arrival of the ignition front. This results in the increased drying of fuel, thereby promoting higher fuel conversion rates, as depicted in Fig. 2(d)–(e). Fig. 4 illustrates the normalised values of fuel bed temperature, ignition front velocity (IFV) and burning rate (BR) for L_l/D=1.00 and 1.48. Values in *Y*-axis in Fig. 4 are obtained by normalizing values of combustion parameters obtained from L_l/D=1.00 case with L_l/D=1.48 case. A significant rise in the values of these parameters can be observed at Q_s/Q_t=0.75 (Fig. 4). In contrast at Q_s/Q_t=0.33 and 0.50, a small difference in the values of fuel bed temperatures, ignition front velocity and burning rate can be observed for L_l/D=1.00 and 1.48. This is as expected, as the flow of secondary air is lower for these cases; hence, the effect of secondary air location (primary freeboard) on fuel conversion is also minimal. The maximum values of burning rate and ignition front velocity were observed for L_l/D=1.00 at Q_s/Q_t=0.75, corresponding to 0.042 kg·m^{-2}·s^{-1} and 0.065 mm·s^{-1}, respectively. Greater values of temperatures for the fuel bed before the arrival of ignition front in the Q_s/Q_t=0.75 case increases the drying process of fuel by removing moisture, thereby promoting higher fuel

Table 4 Fuel bed temperatures and fuel conversion rates for L_l/D=1.00 and 1.48

L_l/mm	L_l/D	Q_p/ kg·m^{-2}·s^{-1}	Q_s/ kg·m^{-2}·s^{-1}	Q_t/ kg·m^{-2}·s^{-1}	Q_s/Q_t	FBT/ °C	IFV/ mm·s^{-1}	BR/ kg·m^{-2}·s^{-1}	Uncertainty
200	1.00	0.089	0.044	0.134	0.33	790	0.058	0.040	FBT: ±1.1% IFV: ±1.0% BR: ±1.2%
			0.089	0.179	0.50	818	0.057	0.040	
			0.179	0.269	0.66	868	0.045	0.034	
			0.224	0.313	0.71	919	0.045	0.036	
			0.269	0.358	0.75	908	0.065	0.042	
300	1.48	0.089	0.044	0.134	0.33	796	0.061	0.040	
			0.089	0.179	0.50	800	0.057	0.038	
			0.179	0.269	0.66	854	0.052	0.036	
			0.224	0.313	0.71	889	0.050	0.037	
			0.269	0.358	0.75	893	0.054	0.037	

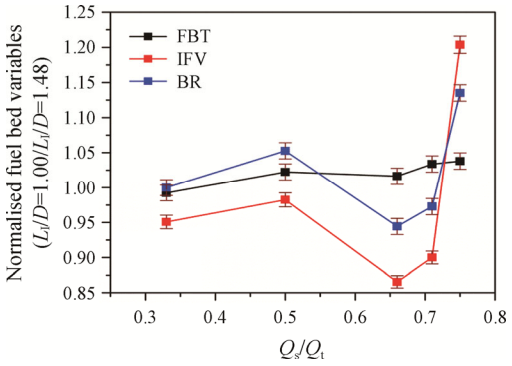

Fig. 4 Normalised values for fuel bed combustion characteristics

conversion in the case of L_l/D=1.00. The values of fuel bed temperatures, burning rate and IFV obtained in current study were in a good agreement with the previous work on the combustion of wood pellets in a batch-type fixed bed combustor [39, 52]. Moreover, comparison of burning rate for L_l/D=1.00 at Q_s/Q_t=0.66 (Q_p=0.089 and Q_s=0.179 kg·m^{-2}·s^{-1}) with previous work [18] at Q_s/Q_t=0.50 (Q_p=0.179 and Q_s=0.179 kg·m^{-2}·s^{-1}) shows that burning rate for the current study was approximately 47.6% lower than in previous work. Despite having the same values for L_l and Q_s, higher values of burning rate in previous study can be linked to the greater value of Q_p (0.179 kg·m^{-2}·s^{-1}), where for sub-stoichiometric conditions, burning rate increases in accordance with the increase in Q_p [50].

3.2 Freeboard temperatures

Fig. 5(a) and 5(b) present the axially resolved centreline temperatures for two primary freeboard lengths and five secondary to total air flow ratios. The results show that the freeboard temperatures to be fairly low for lower Q_s flow rates at Q_s/Q_t=0.33 and 0.50, corresponding to Q_s=0.044 kg·m^{-2}·s^{-1} and 0.089 kg·m^{-2}·s^{-1} (Q_p=0.089 kg·m^{-2}·s^{-1}) for both L_l/D=1.00 and 1.48. This indicates that if a sufficient amount of secondary air is not supplied in the freeboard region, then the influence of primary freeboard length on freeboard temperatures becomes negligible. Adding further secondary air in the case of Q_s/Q_t=0.66, 0.71 and 0.75, corresponding to Q_s=0.179, 0.224 and 0.269 kg·m^{-2}·s^{-1}, significantly increases freeboard temperatures. Similar values of freeboard temperature can be noticed for L_l= 1.00 and 1.48 at Q_s/Q_t=0.33 and 0.50, as seen in Fig. 5(a). For higher values of Q_s/Q_t at 0.66, 0.71 and 0.75, L_l/D=1.00 generally have greater freeboard temperatures in comparison to L_l/D=1.48 cases. The highest temperature in the upstream (x=50 mm) of secondary air in the case of L_l/D=1.00 was observed at Q_s/Q_t=0.75 (839°C), whereas for L_l/D=1.48, the highest freeboard temperature (785°C) in the upstream of secondary air was at Q_s/Q_t=0.71, as illustrated in Fig. 5(b). This indicates that for L_l/D = 1.48, adding more secondary air after Q_s/Q_t=0.71 (Q_s=0.224 kg·m^{-2}·s^{-1}) reduces freeboard temperature. However, for L_l/D=1.00, temperatures were in an increasing trend even at Q_s/Q_t=0.75 (Q_s=0.269 kg·m^{-2}·s^{-1}). This behaviour, in addition to higher freeboard temperatures for L_l/D = 1.00 at Q_s/Q_t=0.75, can be linked to greater values of BR and IFV, as seen in Table 4, as well as fuel bed temperature trends illustrated in Fig. 2, where L_l/D=1.00 had a significant increase for in-fuel bed progress variables at Q_s/Q_t=0.75. Interestingly, between lower and higher freeboard temperature conditions there was an instability case at Q_s=0.134 kg·m^{-2}·s^{-1} and Q_p=0.089 kg·m^{-2}·s^{-1} for Q_s/Q_t=0.60. Freeboard temperature in the upstream of secondary air injection (x=150 mm) for L_l/D=1.00 at Q_s/Q_t=0.66 (Q_s=0.179 kg·m^{-2}·s^{-1}) were approximately 27% less than those observed by Junejo et al. [18] for Q_s/Q_t=0.50 and Q_s=0.179 kg·m^{-2}·s^{-1}. Lower freeboard temperature in the specified case could be a result of a lesser primary air flow rate of 0.089 kg·m^{-2}·s^{-1}, as compared to 0.179 kg·m^{-2}·s^{-1} in the previous study that resulted in lower freeboard temperatures with accompanying lower fuel conversion rates.

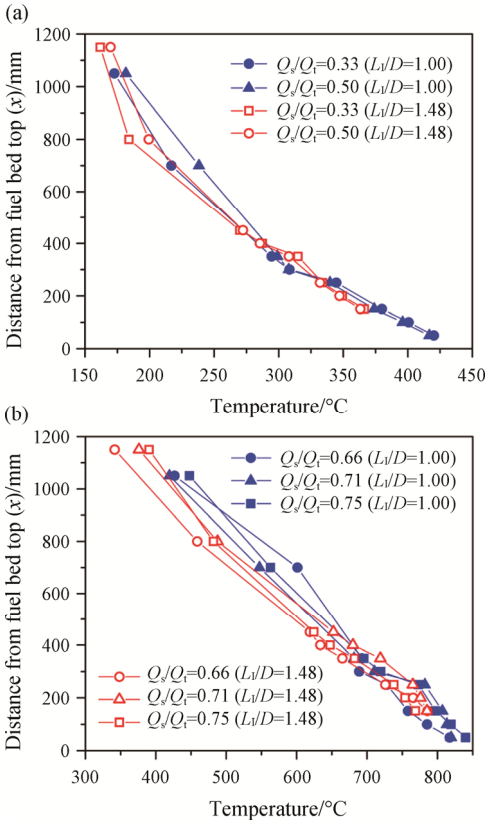

Fig. 5 Centreline freeboard temperatures at (a) Q_s/Q_t=0.33 and 0.50 and (b) Q_s/Q_t=0.66, 0.71 and 0.75 for L_l/D=1.00 and 1.48

3.3 Freeboard gaseous emissions

Table 5 shows the concentration of various gaseous emissions (CO_2, CO and NO_x), whilst Fig. 6 shows the normalised values of these gaseous species for different values of Q_s/Q_t tested at L_l/D=1.00 and 1.48. A rise in Q_s/Q_t from 0.33 to 0.66 leads to higher CO_2 values in the flue gas. CO_2 concentration in the flue gas increased by approximately 37.5% when Q_s/Q_t increased from 0.33 to 0.66 for L_l/D=1.00. Further increasing the Q_s/Q_t from 0.71 to 0.75 had minimal effect on the CO_2 concentration in the flue gas for both L_l/D=1.00 and 1.48. The lower CO_2 concentration in the cases of Q_s/Q_t=0.33 and 0.50 can be linked to lower freeboard temperatures, as well as fuel conversion rates due to lesser secondary air flow rates, as evident in Fig. 5 and Table 4. Higher freeboard temperatures and burning rates were observed for Q_s/Q_t=0.71 and 0.75 due to the availability of sufficient oxygen in the freeboard, which leads to more efficient combustion and an increase in CO_2 values. Moreover, CO_2 concentration was quite similar across all the investigated Q_s/Q_t values for L_l/D=1.00 and 1.48. Interestingly, at L_l/D=1.00 and 1.48, NO_x emissions were significantly greater for lower values of Q_s/Q_t (0.33 and 0.50) as compared to higher values of 0.66, 0.71 and 0.75. These emissions were 564% higher for Q_s/Q_t=0.33 as compared to Q_s/Q_t=0.75 at L_l/D=1.00. Formation of NO_x as a result of biomass combustion can occur due to three mechanisms: (1) thermal NO_x (2) prompt NO_x and (3) fuel NO_x [56]. Thermal NO_x refers to the NO_x produced due to the oxidation of atmospheric nitrogen at very high temperatures. Prompt NO_x is produced due to the presence of hydrocarbon radicals in the fuel and fuel NO_x is produced due to the release of HCN and NHi radicals from nitrogen containing fuels such as biomass during the devolatisation process. In the case of biomass combustion, fuel based NO_x accounts for more than 70% of the total NO_x emissions [57, 58]. Moreover, the formation of thermal and prompt NO_x takes place at very higher combustion temperatures, between 1300°C–1400°C [59]; as maximum combustion temperatures, both in the fuel bed and freeboard, for the current study, were approximately 900°C, the share of fuel based NO_x will be expected to be greater in this study. Furthermore, an uncertainty of 10% in NO_x emissions can be due to the wide range of temperatures (175°C–450°C) observed near the exhaust of the combustor where gaseous emissions were being measured. Additionally, uncertainty in NO_x emissions can also be due to variation in fuel properties (Nitrogen content). The supply of primary air less than stoichiometric condition decreases the fuel bed temperature. Additionally, this also results in an increase in the CO concentration, both of which contribute to lower NO_x emissions [60, 61]. However, since in the current study primary air flow rate was constant in all of the tested conditions, any change in NO_x concentration was primarily due to secondary air flow rate.

As observed in Table 5, CO concentration in flue gas for Q_s/Q_t=0.33 and 0.50 was significantly higher than Q_s/Q_t=0.66, 0.71 and 0.75. Interestingly, concentration of NO_x in the flue gas was slightly lower for L_l/D=1.48 as compared to L_l/D=1.00. This could be due to the condition where at L_l/D=1.00, secondary air was located closer to the fuel bed, in a high temperature region, where the majority of the combustion reactions take place. Therefore, introducing secondary air at this location provides the oxygen required to complete the oxidation of fuel based nitrogen in a high temperature region. The results presented in the current study are also consistent with previous studies on combustion of biomass and coal-biomass blends in fluidized bed reactors [61–63]. NO_x emissions can be reduced significantly by positioning secondary air at a farther position from the fuel bed (L_l/D=1.48), as well as at greater values for Q_s/Q_t of 0.66, 0.71 and 0.75.

Table 5 shows that irrespective of primary freeboard length, CO emissions are significantly affected by Q_s/Q_t,

Table 5 Concertation of CO_2, O_2, NO_x and CO in flue gas corrected at 10% of O_2 for L_l/D=1.00 and 1.48

L_l/ mm	L_l/D	Q_p/ kg·m^{-2}·s^{-1}	Q_s/ kg·m^{-2}·s^{-1}	Q_t/ kg·m^{-2}·s^{-1}	Q_s/Q_t	CO_2/ %	O_2/ %	NO_x/ 10^{-6}	CO/ 10^{-6}	Uncertainty
200	1.00	0.089	0.044	0.134	0.33	7.68	9.91	505	–	CO_2: ±4.3% O_2: ±2.2% NO_x: ±10.9% CO: ±9.8%
			0.089	0.179	0.50	7.61	11.32	450	96 435	
			0.179	0.269	0.66	10.56	6.21	34	1610	
			0.224	0.313	0.71	10.64	9.3	57	341	
			0.269	0.358	0.75	10.57	12.2	76	201	
300	1.48	0.089	0.044	0.134	0.33	7.52	10.16	444	–	
			0.089	0.179	0.50	7.64	13.83	448	97 493	
			0.179	0.269	0.66	9.87	6.18	28	2686	
			0.224	0.313	0.71	10.62	9.55	43	613	
			0.269	0.358	0.75	10.54	13.29	71	278	

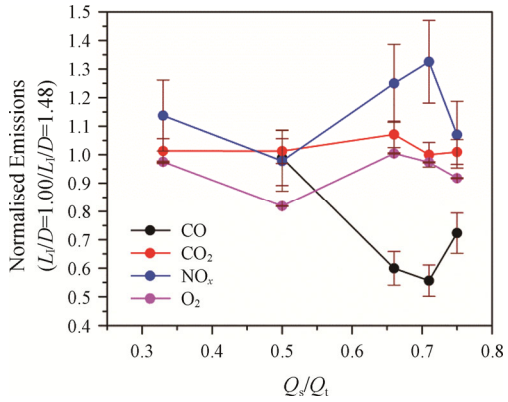

Fig. 6 Normalised gaseous emission species

as increasing Q_s/Q_t from 0.33 to 0.75 significantly reduces CO from 9.6435×10^{-2} to 2.01×10^{-4} (L_l/D=1.00). This significant reduction in CO concentration is also coupled with observations from Figs. 2–5, where higher secondary air flow rates in the case of Q_s/Q_t=0.75 increase both fuel conversion rates and freeboard temperatures. CO emissions were also reduced when secondary air was located closer to the fuel bed at L_l/D= 1.00. This trend was more observable at higher values of Q_s/Q_t, as seen in Fig. 6. Accordingly, CO concentration for Q_s/Q_t=0.33 was very high (>0.125) and therefore, was above the measurement range of the gas analyser. A higher CO concentration in the case of Q_s/Q_t=0.33 could be due to air staged operation of the combustor. Since the primary air supply to the combustor was low (fuel rich), this can result in the generation of CO in large amounts. If the secondary air flow is sufficient, the product of incomplete combustion from the fuel bed, including CO, should combust in the freeboard region. Therefore, at Q_s/Q_t=0.33, lower values of secondary air flow rate (0.089 kg·m^{-2}·s^{-1}) resulted in higher concentration of CO. Further, increase in secondary air supply (Q_s=0.269 kg·m^{-2}·s^{-1}), as indicated by greater values of Q_s/Q_t=0.75, resulted in lower CO concentration. A significant decrease in CO concentration with the increase in Q_s/Q_t has also been documented by the earlier works conducted on combustion of wood pellets [31, 32, 64]. CO emissions in the current study are significant lower than previous work [18], for both L_l/D=1.00 and 1.48. Furthermore, CO concentration for the previous work were approximately 2100% and 1200% higher than current work for L_l/D=1.00 and 1.48 respectively; the higher CO concentration in previous work can be linked to lower secondary air flowrate.

Fig. 7 shows the correlation of downstream freeboard temperature with CO and O_2 concentration in the flue gas. The downstream temperature in Fig. 7 was measured at x=250 mm for L_l/D=1.00. Downstream location of temperature at x=250 in Fig. 7 was selected due to being closer to secondary air, in the higher temperature zone where the combustion of unburnt volatiles occurs. The concentration of O_2 was higher in the exhaust gas, approximately 9.91% and 11.3% for Q_s/Q_t=0.33 and 0.50, respectively. The higher O_2 concentration in these cases was coupled with lower freeboard temperatures and higher CO emissions. This indicates that even though the secondary air supply was low for Q_s/Q_t=0.33 and 0.50, it did not react greatly with the unburnt volatiles emitted from the fuel bed (to convert CO into CO_2), which resulted in higher O_2 and CO concentration. As sufficient Q_s is supplied (Q_s/Q_t=0.66, Q_s=0.179 kg·m^{-2}·s^{-1}), O_2 decreases with a significant increase in freeboard temperature and CO reduction. However, further increasing Q_s/Q_t ratio to 0.71 and 0.75 and Q_s from 0.224 kg·m^{-2}·s^{-1} to 0.269 kg·m^{-2}·s^{-1}, again resulted in higher O_2 concentration due to the supply of excess air in the freeboard, which resulted in higher freeboard temperature and a further reduction in CO.

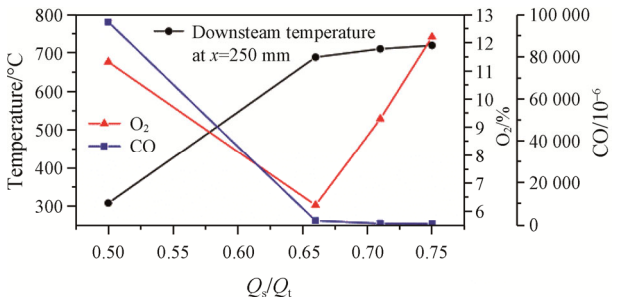

Fig. 7 CO, O_2 and downstream temperature correlation

4. Conclusions

Experiments have been conducted on a laboratory-scale batch-type fixed bed combustor to characterise the influence of primary freeboard length (L_l) and secondary air flow rate on burning rate and temperature distribution in the fuel bed as well in the freeboard region. Concentration of gaseous emissions (CO_2, NO_x, CO) was also investigated. These experiments were conducted at two different primary freeboard lengths of 200 mm (L_l/D=1.00) and 300 mm (L_l/D=1.48), using five different secondary to total air ratios (Q_s/Q_t) ranging from 0.33 to 0.75 at a constant primary air flowrate of 0.089 kg·m^{-2}·s^{-1}. The following conclusions are drawn:

Fuel Bed Temperatures and Conversion: An increase in secondary to total air ratio (Q_s/Q_t) from 0.33 to 0.75 results in higher fuel bed temperatures. Variation in primary freeboard length had minimal effect on fuel bed temperatures. No significant effect of Q_s/Q_t on fuel conversion rates (BR and IFV) was observed for primary freeboard lengths of L_l/D=1.00 and 1.48 at Q_s/Q_t=0.33

and 0.50. However, as Q_s/Q_t increased to 0.71 and 0.75, a rise in fuel conversion rates was observed. The effect of primary freeboard length on fuel conversion rates was more prominent at Q_s/Q_t=0.75, where L_l/D=1.00 possessed marginally higher values of BR in comparison to L_l/D=1.48. A greater fuel conversion rate for Q_s/Q_t= 0.75 at L_l/D=1.00 can be attributed to the drying of the fuel caused by heat transfer from ignition front to the bottom layers of fuel bed due to stronger secondary air flow rate.

Freeboard Temperatures: Freeboard temperature was found to have a positive correlation with Q_s/Q_t. Maximum freeboard temperatures were found in the vicinity of secondary air injection and at Q_s/Q_t=0.75 for L_l/D=1.00 and at Q_s/Q_t=0.71 for L_l/D=1.48. Freeboard temperatures were very similar for L_l/D=1.00 and 1.48 at Q_s/Q_t=0.33 and 0.50. However, as the Q_s/Q_t increased to 0.66, 0.71 and 0.75, L_l/D=1.00 had higher freeboard temperatures than L_l/D=1.48.

Emissions: An increase in Q_s/Q_t from 0.33 to 0.75 resulted in lower CO and NO_x emissions with accompanying higher CO_2 concentration in the flue gas. For higher values of Q_s/Q_t, i.e. 0.71 and 0.75, significantly lower CO emissions were observed attributing towards the complete combustion of volatiles (consequence of higher freeboard temperature) in the freeboard region. Injecting secondary air at a higher position at L_l/D=1.48 from fuel bed results in lower NO_x emissions as compared to L_l/D=1.00. However, this reduction in NO_x is accompanied with higher CO emissions.

Overall, the combustion characteristics were influenced by both the secondary to total air ratio and primary freeboard length. Fuel bed temperatures, fuel conversion rate, freeboard temperatures and emissions (CO) were found to be lower in the current work as compared to previous work conducted on the same combustor but at a varied primary air flow rate. The outcomes from the current work complements the available data in effective designing and a better understanding of the combustion and emissions of biomass fuels in large commercial scale moving grate combustors.

Conflict of Interest

On behalf of all authors, the corresponding author states that there is no conflict of interest.

Funding note

Open Access funding enabled and organized by CAUL and its Member Institutions.

Electronic Supplementary Materials

Supplementary materials are available in the online version of this article at https://doi.org/10.1007/s11630-023-1869-9.

References

[1] Hai I.U., Sher F., Yaqoob A., et al., Assessment of biomass energy potential for SRC willow woodchips in a pilot scale bubbling fluidized bed gasifier. Fuel, 2019. 258: 116143.

[2] Qureshi Y., Ali U., Sher F., Part load operation of natural gas fired power plant with CO_2 capture system for selective exhaust gas recirculation. Applied Thermal Engineering, 2021, 190: 116808. DOI: 10.1016/j.applthermaleng.2021.116808.

[3] Yin C., Qiu S.X., Zhang S.F., et al., Strength degradation mechanism of iron coke prepared by mixed coal and Fe_2O_3. Journal of Analytical and Applied Pyrolysis, 2020, 150: 104897. DOI: 10.1016/j.jaap.2020.104897.

[4] Cai S.S., Zhang S.F., Wei Y.Y., et al., A novel method for removing organic sulfur from high-sulfur coal: Migration of organic sulfur during microwave treatment with NaOH-H_2O_2. Fuel, 2021, 289: 119800. DOI: 10.1016/j.fuel.2020.119800.

[5] Caposciutti G., Barontini F., Antonelli M., et al., Experimental investigation on the air excess and air displacement influence on early stage and complete combustion gaseous emissions of a small scale fixed bed biomass boiler. Applied Energy, 2018, 216: 576–587. DOI: 10.1016/j.apenergy.2018.02.125.

[6] Nicoletti G., Arcuri N., Nicoletti G., et al., A technical and environmental comparison between hydrogen and some fossil fuels. Energy Conversion and Management, 2015, 89: 205–213. DOI: 10.1016/j.enconman.2014.09.057.

[7] Farzad S., Mandegari M.A., Gorgens J.F., A critical review on biomass gasification, co-gasification, and their environmental assessments. Biofuel Research Journal, 2016, 3(4): 483–495. DOI: 10.18331/BRJ2016.3.4.3.

[8] Ullah S., Noor R.S., Sanaullah, et al., Analysis of biofuel (briquette) production from forest biomass: a socioeconomic incentive towards deforestation. Biomass Conversion and Biorefinery, 2023, 13: 1–15. DOI: 10.1007/s13399-021-01311-5.

[9] Kummamuru B., WBA global bioenergy statistics 2017. World Bioenergy Association, 2016.

[10] McKendry P., Energy production from biomass (Part 2): Conversion technologies. Bioresource Technology, 2002, 83(1): 47–54. DOI: 10.1016/S0960-8524(01)00119-5.

[11] Yin C., Rosendahl L.A., Kaer S.K., Grate-firing of

biomass for heat and power production. Progress in Energy and Combustion Science, 2008, 34(6): 725–754. DOI: 10.1016/j.pecs.2008.05.002.

[12] Khodaei H., Al-Abdeli Y.M., Guzzomi F., et al., An overview of processes and considerations in the modelling of fixed-bed biomass combustion. Energy, 2015, 88: 946–972. DOI: 10.1016/j.energy.2015.05.099.

[13] Yokoyama S., Matsumura Y., The Asian biomass handbook: a guide for biomass production and utilization. The Japan Institute of Energy, 2008, pp. 61–62.

[14] Wurzenberger J.C., Wallner S., Raupenstrauch H., et al., Thermal conversion of biomass: Comprehensive reactor and particle modeling. AIChE Journal, 2002, 48(10): 2398–2411. DOI: 10.1002/aic.690481029.

[15] Chaney J., Liu H., Li J.X., An overview of CFD modelling of small-scale fixed-bed biomass pellet boilers with preliminary results from a simplified approach. Energy Conversion and Management, 2012, 63: 149–156. DOI: 10.1016/j.enconman.2012.01.036.

[16] Chhiti Y., Kemiha M., Thermal conversion of biomass, pyrolysis and gasification: A review. International Journal of Engineering and Science (IJES), 2013, 2(3): 75–85.

[17] Yang Y.B., Ryu C., Khor A., et al., Effect of fuel properties on biomass combustion. Part II. Modelling approach—identification of the controlling factors. Fuel, 2005, 84(16): 2116–2130. DOI: 10.1016/j.fuel.2005.04.023.

[18] Junejo A., Al-Abdeli Y.M., Porteiro J., Role of primary freeboard on staged combustion of hardwood pellets in a fixed bed combustor. Bioenergy Research, 2022. DOI: 10.1007/s12155-022-10504-3.

[19] Deng M., Li P.C., Shan M., et al., Optimizing supply airflow and its distribution between primary and secondary air in a forced-draft biomass pellet stove. Environmental Research, 2020, 184: 109301. DOI: 10.1016/j.envres.2020.109301.

[20] Rashidian B., Al-Abdeli Y.M., Patiño D., et al., Effect of freeboard deflectors in the fixed bed combustion of biomass. Applied Thermal Engineering, 2016, 103: 543–552. DOI: 10.1016/j.applthermaleng.2016.04.140.

[21] Rashid T., Taqvi S.A.A., Sher F., et al., Enhanced lignin extraction and optimisation from oil palm biomass using neural network modelling. Fuel, 2021, 293: 120485. DOI: 10.1016/j.fuel.2021.120485.

[22] Rashid T., Sher F., Rasheed T., et al., Evaluation of current and future solvents for selective lignin dissolution-A review. Journal of Molecular Liquids, 2021, 321: 114577. DOI: 10.1016/j.molliq.2020.114577.

[23] Nazir M.H., Ayoub M., Zahid I., et al., Waste sugarcane bagasse-derived nanocatalyst for microwave-assisted transesterification: Thermal, kinetic and optimization study. Biofuels, Bioproducts and Biorefining, 2022, 16(1): 122–141.

[24] Zulqarnain, Yusoff M.H.M., Ayoub M., et al., Solvent extraction and performance analysis of residual palm oil for biodiesel production: Experimental and simulation study. Journal of Environmental Chemical Engineering, 2021, 9(4): 105519. DOI: 10.1016/j.jece.2021.105519.

[25] Michopoulos A., Skoulou V., Voulgari V., et al., The exploitation of biomass for building space heating in Greece: Energy, environmental and economic considerations. Energy Conversion and Management, 2014, 78: 276–285. DOI: 10.1016/j.enconman.2013.10.055.

[26] Tchapda A.H., Pisupati S.V., A review of thermal co-conversion of coal and biomass/waste. Energies, 2014. 7(3): 1098–1148. DOI: 10.3390/en7031098.

[27] Yin C.G., Rosendahl L., Kær S.K., et al., Mathematical modeling and experimental study of biomass combustion in a thermal 108 MW grate-fired boiler. Energy & Fuels, 2008, 22(2): 1380–1390. DOI: 10.1021/ef700689r.

[28] Wiinikka H., Gebart R., Critical parameters for particle emissions in small-scale fixed-bed combustion of wood pellets. Energy & Fuels, 2004, 18(4): 897–907. DOI: 10.1021/ef030173k.

[29] Nussbaumer T., Combustion and co-combustion of biomass: fundamentals, technologies, and primary measures for emission reduction. Energy & Fuels, 2003, 17(6): 1510–1521. DOI: 10.1021/ef030031q.

[30] Khodaei H., Guzzomi F.G., Patino D., et al., Air staging strategies in biomass combustion-gaseous and particulate emission reduction potentials. Fuel Processing Technology, 2017, 157: 29–41. DOI: 10.1016/j.fuproc.2016.11.007.

[31] Zadravec T., Rajh B., Kokalj F., et al., Influence of air staging strategies on flue gas sensible heat losses and gaseous emissions of a wood pellet boiler: An experimental study. Renewable Energy, 2021, 178: 532–548. DOI: 10.1016/j.renene.2021.05.150.

[32] Collado R., Monedero E., Casero-Alonso V.M., et al., Almond shells and exhausted olive cake as fuels for biomass domestic boilers: Optimization, performance and pollutant emissions. Sustainability, 2022, 14(12): 7271. DOI: 10.3390/su14127271.

[33] Lamberg H., Sippula O., Tissari J., et al., Effects of air staging and load on fine-particle and gaseous emissions from a small-scale pellet boiler. Energy & Fuels, 2011, 25(11): 4952–4960. DOI: 10.1021/ef2010578.

[34] Pérez-Orozco R., Patiño D., Porteiro J., et al., Bed cooling effects in solid particulate matter emissions during biomass combustion. A morphological insight. Energy, 2020, 205: 118088.

[35] Regueiro A., Patiño D., Porteiro J., et al., Effect of air staging ratios on the burning rate and emissions in an underfeed fixed-bed biomass combustor. Energies, 2016, 9(11): 940. DOI: 10.3390/en9110940.

[36] Kirch T., Birzer C.H., Medwell P.R., et al., The role of primary and secondary air on wood combustion in cookstoves. International Journal of Sustainable Energy, 2018, 37(3): 268–277. DOI: 10.1080/14786451.2016.1166110.

[37] Junejo A., Al-Abdeli Y., Porteiro J., Freeboard effects on instabilities in a fixed bed biomass combustor. Proceedings of the Australian Combustion Symposium 2021, Australia and New Zealand section of the Combustion Institute, Toowoomba, Queensland.

[38] Junejo A., Al-Abdeli Y.M., Ikhlaq M., Progress variables to resolve the steady state period in a batch-type fixed bed combustor. Combustion Science and Technology, 2022, pp. 1–23. DOI: 10.1080/00102202.2022.2150969.

[39] Porteiro J., Patiño D., Miguez J.L., et al., Study of the reaction front thickness in a counter-current fixed-bed combustor of a pelletised biomass. Combustion and Flame, 2012. 159(3): 1296–1302. DOI: 10.1016/j.combustflame.2011.10.007.

[40] Khodaei H., Al-Abdeli Y.M., Guzzomi F., et al., An overview of processes and considerations in the modelling of fixed-bed biomass combustion. Energy, 2015, 88: 946–972. DOI: 10.1016/j.energy.2015.05.099.

[41] Khan A.A., Aho M., de Jong W., et al., Scale-up study on combustibility and emission formation with two biomass fuels (B quality wood and pepper plant residue) under BFB conditions. Biomass and Bioenergy, 2008, 32(12): 1311–1321. DOI: 10.1016/j.biombioe.2008.03.011.

[42] Mami M.A., Mätzing H., Gehrmann H.J., et al., Investigation of the olive mill solid wastes pellets combustion in a counter-current fixed bed reactor. Energies, 2018, 11(8): 1965. DOI: 10.3390/en11081965.

[43] Engineers A.S.O.M., Flue and exhaust gas analysis, ASME Power Test Code 19.10. 1981, ASME, New York, USA.

[44] Lundgren J., Hermansson R., Dahl J., Experimental studies of a biomass boiler suitable for small district heating systems. Biomass and Bioenergy, 2004, 26(5): 443–453. DOI: 10.1016/j.biombioe.2003.09.001.

[45] ASTM E871-82(2019), Standard test method for moisture analysis of particulate wood fuels. 2019, ASTM International West Conshohocken, PA.

[46] ASTM E872-82(2019), Standard test method for volatile matter in the analysis of particulate wood fuels. 2019, ASTM International West Conshohocken, PA.

[47] ASTM D1102-84(2021), Standard test method for ash in wood. 2021, ASTM International West Conshohocken, PA.

[48] ASTM D5865(2007), A standard test method for gross calorific value of coal and coke. ASTM International West Conshohocken, PA.

[49] ASTM E873-82(2019), Standard test method for bulk density of densified particulate biomass fuels. 2019, ASTM International West Conshohocken, PA.

[50] Porteiro J., Patiño D., Moran J., et al., Study of a fixed-bed biomass combustor: Influential parameters on ignition front propagation using parametric analysis. Energy & Fuels, 2010, 24(7): 3890–3897. DOI: 10.1021/ef100422y.

[51] Elorf A., Asbik B.M., Sarh B., et al., Fixed-bed biomass combustor: Air mass flow rate and particles size effects on ignition front propagation of solid olive waste. Combustion Science and Technology, 2022, 194: 365–377.

[52] Porteiro J., Patiño D., Collazo J., et al., Experimental analysis of the ignition front propagation of several biomass fuels in a fixed-bed combustor. Fuel, 2010, 89(1): 26–35. DOI: 10.1016/j.fuel.2009.01.024.

[53] Kirch T., Birzer C.H., van Eyk P.J., et al., Influence of primary and secondary air supply on gaseous emissions from a small-scale staged solid biomass fuel combustor. Energy & Fuels, 2018, 32(4): 4212–4220. DOI: 10.1021/acs.energyfuels.7b03152.

[54] Horttanainen M., Saastamoinen J., Sarkomaa P., Operational limits of ignition front propagation against airflow in packed beds of different wood fuels. Energy & Fuels, 2002, 16(3): 676–686. DOI: 10.1021/ef010209d.

[55] Yang Y.B., Sharifi V.N., Swithenbank J., Effect of air flow rate and fuel moisture on the burning behaviours of biomass and simulated municipal solid wastes in packed beds. Fuel, 2004, 83(11–12): 1553–1562. DOI: 10.1016/j.fuel.2004.01.016.

[56] Lin J.J., Wang Q.H., Liang X.R., et al., Investigation on fuel-N transformation properties of coal/biomass heating process in CO_2 atmosphere. Journal of Thermal Science, 2021, 30(4): 1141–1150. DOI: 10.1007/s11630-021-1474-8.

[57] Mousavi S.M., Fatehi H., Bai X.S., Numerical study of the combustion and application of SNCR for NO_x reduction in a lab-scale biomass boiler. Fuel, 2021, 293: 120154. DOI: 10.1016/j.fuel.2021.120154.

[58] Williams A., Jones J.M., Ma L., et al., Pollutants from the combustion of solid biomass fuels. Progress in Energy and Combustion Science, 2012, 38(2): 113–137. DOI: 10.1016/j.pecs.2011.10.001.

[59] Glarborg P., Jensen A., Johnsson J.E., Fuel nitrogen conversion in solid fuel fired systems. Progress in energy and combustion science, 2003, 29(2): 89–113. DOI: 10.1016/S0360-1285(02)00031-X.

[60] Aarna I., Suuberg E.M., The role of carbon monoxide in the NO-carbon reaction. Energy & Fuels, 1999, 13(6): 1145–1153.

[61] Sher F., Pans M.A., Afilaka D.T., et al., Experimental investigation of woody and non-woody biomass combustion in a bubbling fluidised bed combustor focusing on gaseous emissions and temperature profiles. Energy, 2017, 141: 2069–2080.
DOI: 10.1016/j.energy.2017.11.118.

[62] Varol M., Atimtay A.T., Olgun H., Emission characteristics of co-combustion of a low calorie and high-sulfur-lignite coal and woodchips in a circulating fluidized bed combustor: Part 2. Effect of secondary air and its location. Fuel, 2014, 130: 1–9.
DOI: 10.1016/j.fuel.2014.04.002.

[63] Saikaew T., Supudommak P., Mekasut L., et al., Emission of NO_x and N_2O from co-combustion of coal and biomasses in CFB combustor. International Journal of Greenhouse Gas Control, 2012, 10: 26–32.
DOI: 10.1016/j.ijggc.2012.05.014.

[64] Houshfar E., Lovas T., Skreiberg O., Detailed chemical kinetics modeling of NO_x reduction in combined staged fuel and staged air combustion of biomass. 18th European Biomass Conference and Exhibition, Lyon, France, 2010.
DOI: 10.5071/18THEUBCE2010-VP2.4.4.